# Increased surface P2X4 receptor regulates anxiety and memory in P2X4 internalization-defective knock-in mice

Eléonore Bertin, Thomas Deluc, Kjara Pilch, Audrey Martinez, Johan-Till Pougnet, Evelyne Doudnikoff, Anne-Emilie Allain, Philine Bergmann, Marion Russeau, Estelle Toulmé, et al.

This is a post-peer-review pre-copyedit version of an article published in Molecular Psychiatry. The final authenticated version is available online at http://dx.doi.org/10.1038/s41380-019-0641-8

# Increased surface P2X4 receptor regulates anxiety and memory in P2X4 internalization-defective knock-in mice

Eléonore Bertin[1,2,8], Thomas Deluc[1,2,3,8], Kjara S. Pilch[1,2,8], Audrey Martinez[1,2], Johan-Till Pougnet[1,2], Evelyne Doudnikoff[1,2], Anne-Emilie Allain[4,5], Philine Bergmann[6], Marion Russeau[7], Estelle Toulmé[1,2], Erwan Bezard[1,2], Friedrich Koch-Nolte[6], Philippe Séguéla[3], Sabine Lévi[7], Bruno Bontempi[1,2], François Georges[1,2], Sandrine S. Bertrand[4,5], Olivier Nicole[1,2] and Eric Boué-Grabot[1,2*]

[1] Univ. de Bordeaux, Institut des Maladies Neurodégénératives, UMR 5293, F-33000 Bordeaux, France
[2] CNRS, Institut des Maladies Neurodégénératives, UMR 5293, F-33000 Bordeaux, France
[3] Department of Neurology and Neurosurgery, Montreal Neurological Institute, Alan Edwards Centre for Research on Pain, McGill University, Montreal, Quebec H3A 2B4, Canada
[4] Univ. de Bordeaux, Institut de Neurosciences Cognitives et Intégratives d'Aquitaine, UMR5287, F-33000 Bordeaux, France
[5] CNRS, Institut de Neurosciences Cognitives et Intégratives d'Aquitaine, UMR5287, F-33000 Bordeaux, France
[6] Institute of Immunology, University Medical Center Hamburg-Eppendorf, Martinistr. 52, D-20246 Hamburg, Germany
[7] INSERM UMR-S 1270, Sorbonne Université, Institut du Fer à Moulin, 75005, Paris, France

[8]: These authors should be considered as co-first authors.

*: Corresponding author: Eric Boué-Grabot (EB-G) Institut des Maladies Neurodégénératives (IMN) CNRS UMR 5293, Université de Bordeaux, 146 rue Léo Saignat, 33076 Bordeaux cedex, France; phone: 33 (0)5 33 51 47 95; email: eric.boue-grabot@u-bordeaux.fr

Short/running title: Increased surface P2X4 alters plasticity and behavior

## Abstract

ATP signaling and surface P2X4 receptors are upregulated selectively in neurons and/or glia in various CNS disorders including anxiety, chronic pain, epilepsy, ischemia and neurodegenerative diseases. However, the cell-specific functions of P2X4 in pathological contexts remain elusive. To elucidate P2X4 functions, we created a conditional transgenic knock-in P2X4 mouse line (Floxed P2X4mCherryIN) allowing the Cre activity-dependent genetic swapping of the internalization motif of P2X4 by the fluorescent mCherry protein to prevent constitutive endocytosis of P2X4. By combining molecular, cellular, electrophysiological and behavioral approaches, we characterized two distinct knock-in mouse lines expressing non-internalized P2X4mCherryIN either exclusively in excitatory forebrain neurons or in all cells natively expressing P2X4. The genetic substitution of wild-type P2X4 by non-internalized P2X4mCherryIN in both knock-in mouse models did not alter the sparse distribution and subcellular localization of P2X4 but increased the number of P2X4 receptors at the surface of the targeted cells mimicking the pathological increased surface P2X4 state. Increased surface P2X4 density in the hippocampus of knock-in mice altered LTP and LTD plasticity phenomena at CA1 synapses without affecting basal excitatory transmission. Moreover, these cellular events translated into anxiolytic effects and deficits in spatial memory. Our results show that increased surface density of neuronal P2X4 contributes to synaptic deficits and alterations in anxiety and memory functions consistent with the implication of P2X4 in neuropsychiatric and neurodegenerative disorders. Furthermore, these conditional P2X4mCherryIN knock-in mice will allow exploring the cell-specific roles of P2X4 in various physiological and pathological contexts.

## Introduction

The release and extracellular action of ATP are a widespread mechanism for cell-to-cell communication in living organisms through activation of P2X and P2Y receptors expressed at the cell surface of most tissues, including the nervous system[1]. Several P2X receptors (P2X) are expressed in the central nervous system (CNS) with varying distributions in neurons as well as in glia[2-4]. P2X receptors are ATP-gated cation channels and their activation by ATP, co-released by neurons with other neurotransmitters[5, 6] or released as a gliotransmitter by astrocytes[7-9], has profound modulatory actions at synapses[1, 10, 11]. Among the seven P2X subunits, P2X4 displays high calcium permeability[12, 13] and a widespread distribution in CNS neurons and glial cells as well as in peripheral tissues[14-16]. Nevertheless P2X4 expression in the brain is sparse[15] and its contribution to the synaptic modulation in normal conditions remains debated[17, 18]. A growing body of evidence suggests that upregulated P2X4 expression plays important roles in various CNS disorders including chronic pain and neurodegenerative diseases such as Alzheimer's disease (AD) or amyotrophic lateral sclerosis (ALS)[19-26]. In the healthy organism, P2X4 is constitutively internalized by the interaction between the adaptor protein 2 (AP2) and a non-canonical endocytosis motif in the C-tail of P2X4 subunit[27, 28]. As a result, P2X4 is found preferentially in intracellular compartments ensuring a low surface expression not only in neurons, but also in microglia and macrophages [29-32]. Intracellular P2X4 may promote vesicle fusion of endosomes or lysosomes [32, 33]. Importantly, intracellular P2X4 pools can be mobilized and trafficked to the cell surface[31, 34], consistent with the critical role of increased P2X4 surface expression in pathological states[19, 21, 24-26, 35-37]. The specific increase in P2X4 expression and surface trafficking in spinal microglia is critical for the pathogenesis of chronic pain[24, 38-41]. Increased P2X4 expression and surface density in neurons has

been observed in the hippocampus or in the spinal cord of AD or ALS mouse models, respectively, suggesting that upregulated P2X4 may contribute to synaptic dysfunction and/or cell death in AD or ALS[23, 25, 26, 35]. However, the extent of the upregulated surface P2X4 state and the cell-specific functions of P2X4 in the pathological context remain elusive.

Here we report the development of conditional knock-in (P2X4mCherryIN) mice mimicking a pathological increase of surface P2X4. We show that the increase of P2X4 at the surface of excitatory neurons decreases anxiety, impairs memory processing, and alters activity-dependent synaptic plasticity phenomena in the hippocampus suggesting that upregulation of neuronal P2X4 observed in AD[25] may have key roles in AD pathogenesis. Overall, we provide an innovative knock-in P2X4 model to study the functional contributions of upregulated P2X4 in specific cells of the nervous system but also in peripheral tissues throughout the body.

## Materials and methods

### Experimental model

The *P2rx4* conditional knock-in mouse line was established at the MCI/ICS (Mouse Clinical Institute, France). *Xenopus* oocytes were isolated as described[42, 43]. Cultures of hippocampal neurons were prepared as described[44] with some modifications. Peritoneal cells were isolated as described [45] (see Supplementary information).

### Ethics approval

All experimental procedures complied with official European guidelines for the care and use of laboratory animals (Directive 2010/63/UE).

**Immunofluorescence and microscopy**

Immunofluorescence studies of neurons, macrophages, brain immunohistochemistry and image acquisition are described in the Supplement and electron microscopy was performed as previously described[46] (see Supplementary information).

**Biotinylation assays and immunoblotting**

Surface biotinylation experiments were performed as described previously[8, 43, 47] from injected *Xenopus* oocytes, mouse peritoneal macrophages and hippocampal cell cultures (see Supplementary information).

**Electrophysiology**

Extracellular field recordings and induction of synaptic plasticity in hippocampal brain slices are described in the Supplement. Two-electrode voltage-clamp recordings from Xenopus oocyte were performed as previously described (see Supplementary information).

**Mouse behavior**

Open field procedure, novel object recognition test[48, 49], elevated plus maze[50], the Y-maze two-trial procedure[51] and spatial memory testing conducted in an 8-arm radial maze are described in the Supplementary information.

**Quantification and statistical analysis**

The number of independent experiments or animals (n), the statistical test used for comparison and the statistical significance (p values) are specified for each Figure panel in the corresponding figure legend. Data are presented as mean ± s.e.m. Data were analyzed and graphs were generated using GraphPad Prism.

## Results

### Substitution of the internalization motif of P2X4 by mCherry protein increases surface density of functional P2X4 receptors

Mutation or ablation of the endocytosis motif of P2X4 ($Y^{378}$xxGL) was previously shown to increase the surface trafficking of P2X4 without altering its functional properties[28, 43]. We generated a P2X4mCherryIN construct in which the endocytosis motif of mouse wild-type (WT) P2X4 was suppressed by swapping the last 11 amino acids in the C-tail of P2X4 with the sequence coding for the red fluorescent protein mCherry (Fig. 1a). ATP-evoked currents recorded from P2X4WT or P2X4mCherryIN expressing *Xenopus* oocytes (Fig. 1b) showed that P2X4mCherryIN response amplitudes were significantly larger than those recorded from P2X4WT (Fig. 1b). We next examined the surface level of P2X4WT and P2X4mCherryIN by biotinylation assays and western blotting from oocytes (Fig. 1c,d). Anti-P2X4 antibodies allowed the detection of P2X4WT (70 kDa) but not P2X4mCherryIN (the anti-P2X4 epitope (amino acids 370-388) is deleted in P2X4mCherryIN constructs). P2X4mCherryIN was detected using anti-RFP antibodies showing a band at 100 kDa in agreement with the fusion of mCherry (30 kDa) to P2X4 (Fig. 1c). Surface/total protein ratio showed that P2X4mCherryIN is more effectively translocated to the surface than P2X4WT in *Xenopus* oocytes (Fig. 1d, $p<0.05$).

We next transfected hippocampal neurons and Cos cells (Fig. 1e-h and supplementary Fig. S1a-d) with extracellularly tagged HA-P2X4WT and HA-P2X4mCherryIN to visualize surface P2X4 on living cells using anti-HA antibodies. Total HA-P2X4 was revealed after cell permeabilization using anti-P2X4 antibodies while the endogenous fluorescence of mCherry fused to P2X4 allowed for direct visualization. HA-P2X4WT is weakly expressed at the surface and is found mainly in intracellular puncta restricted to the soma and proximal dendrites of neurons[27]. In contrast, HA-P2X4mCherryIN was ~10 times more expressed at the surface of neurons. Surface P2X4mCherryIN puncta are uniformly distributed at the surface including distal dendrites. Co-staining with the post-synaptic marker Homer-1c-GFP revealed that surface P2X4mCherryIN are equally distributed in small extrasynaptic clusters and in larger clusters

juxtaposed to synapses (Fig. 1g,h and supplementary Fig. S1d). Finally, we confirmed the predominant intracellular localization of untagged P2X4WT in mouse transfected hippocampal neurons using Nodu-246, a rat monoclonal antibody recognizing the native extracellular domain of mouse P2X4 [52], whereas P2X4mCherryIN is highly and uniformly distributed at the cell surface (Fig. 1i).

**Generation of knock-in mice with non-internalized P2X4mCherryIN and expression in the brain**

We generated the conditional floxed P2X4mCherryIN knock-in mice (Floxed) by homologous recombination using a targeting vector (see Fig. 2a) designed to flox the last 4 exons (exons 9 to 12) of *P2rx4* allele (P2X4 internalization motif being located on exons 11 and 12) and followed by the insertion of a DNA fragment corresponding to the fusion of exons 9, 10 and partially 11 with mCherry cDNA. We next generated CMVCre$^{+}$-P2X4mCherryIN$^{F/F}$ (namely CMV) mice and CaMK2Cre$^{+}$-P2X4mCherryIN $^{F/F}$ (CaMK2) mice by breeding Floxed mice with mice either expressing the Cre recombinase under the cytomegalovirus (CMV-Cre) or the calmodulin kinase 2 (CaMK2-Cre) promoter (supplementary Fig. S2). Cre-dependent excision of floxed P2X4mCherryIN allele would lead to the replacement of P2X4WT by non-internalized P2X4mCherryIN. It is important to note that excised *p2rx4* gene remains under the control of its own promoter, thus P2X4mCherryIN will replace P2X4WT only in cells expressing natively P2X4 without altering its distribution pattern or its expression level. In CMV mice, where a Cre-dependent excision occurs in all cells, P2X4mCherryIN would replace P2X4WT in all cells natively expressing P2X4 throughout the body. In CaMK2 mice, substitution of P2X4WT by P2X4mCherryIN is expected to be restricted to excitatory forebrain neurons natively expressing P2X4, while other P2X4 expressing cells such as glial cells and other neuronal types express P2X4WT. Homozygous Floxed, CMV and CaMK2 mice were used in all the following experiments and were viable, normal in size or weight reproduced normally and displayed no obvious physical or behavioral abnormalities (see Supplementary information).

Reverse transcription (RT)-PCR in different brain regions from the different mice showed that Floxed mice solely expressed P2X4WT mRNA while CMV mice only expressed P2X4mCherryIN mRNA (Fig. 2c). As expected, CaMK2 mice expressed both wild-type and knock-in mRNAs since only a subset of

P2X4 expressing cells (forebrain excitatory neurons) replace P2X4WT by P2X4mCherryIN. Next, we tested P2X4mCherryIN expression in the brain on a protein level (Fig. 2d-f). The sparse expression of P2X4 throughout the brain observed in previous works[3, 53] was recently confirmed using tdTomato *p2xr4* reporter mice in which the detection of cytosolic tdTomato-expressing cells required the use of anti-tdTomato antibodies[15]. Not surprisingly, endogenous fluorescence of mCherry fused to P2X4 was not directly visible on brain slices of the different knock-in mice but could be visualized using anti-RFP antibodies. P2X4mCherryIN was detected in the pyramidal neuron layer of the hippocampus and in the soma of neurons throughout the cortex[3, 15] in both CMV and CaMK2, but not in Floxed or P2X4 knockout (P2X4KO) mice (Fig. 2d). In addition, we confirmed the abundant expression of P2X4mCherryIN in the epithelial glomerular layer of the olfactory bulb[15, 54] as well as a moderate presence in cerebellar Purkinje cells[3, 15] of CMV mice but not of CaMK2 mice, as expected. These results showed that P2X4mCherryIN distribution in CMV mice is similar to that of P2X4 in wild-type mice[15] and the restricted detection of P2X4mCherryIN in forebrain neurons in CaMK2 mice confirmed the specificity of Cre-dependent excision. (supplementary Fig. S3a-b). The detection of a 100 kDa band with anti-RFP antibodies in western blots of total proteins from different brain regions confirmed the substitution of P2X4WT by P2X4mCherryIN in CMV mice (Fig. 2e). The absence of detection of P2X4mCherryIN in CaMK2 mice indicated that the replacement of P2X4WT by P2X4mCherryIN is more widespread in the CMV than in CaMK2 mice, as expected. Moreover, the absence of detection of P2X4WT in Floxed or CaMK2 mice with anti-P2X4 confirmed the sparse P2X4 expression in the brain tissues (Fig. 2e).

Electron microscopy (E.M.) of anti-RFP labeling in hippocampal CA1 region or cortex revealed that P2X4mCherryIN was present at postsynaptic sites of excitatory synapses, preferentially at the edge of the postsynaptic density (Fig. 2f). At some asymmetric excitatory synapses, P2X4mCherryIN was located at both pre- and post-synaptic sites (Fig. 2f) and also found intracellularly in association with the endoplasmic reticulum membranes or occasionally with mitochondria (supplementary Fig. S3c). This suggests that replacement of P2X4WT by P2X4mCherryIN does not alter its subcellular distribution [3]. The identification of symmetric synapses on morphological criteria being difficult, the presence of P2X4 at GABAergic synapses was not confirmed in CMV mice. In contrast, E.M. analysis revealed the

presence of P2X4mCherryIN in astrocytes of CMV mice in the astrocyte end-feet encircling endothelial cells (Supplementary Fig. S3d).

**Endogenous P2X4mCherryIN fluorescence is directly observable in macrophages or after LPS-induced *de novo* expression in microglia of CMV mice**

In mice, *de novo* P2X4 expression was observed in spinal microglia after nerve injury or in the brain after intracerebral lipopolysaccharide (LPS) injection in tdTomato *P2xr4* reporter mice [15, 38, 39, 41, 55]. We performed *in vivo* LPS microinjections into the hippocampus of CMV, CaMK2, Floxed and P2X4KO mice and examined P2X4mCherryIN fluorescence (Fig. 3 and supplementary Fig. S4). In control saline-injected mice, no endogenous mCherry fluorescence was visible in the hippocampus of all mouse genotypes and only a faint staining was revealed for the microglial marker Iba1 (Fig. 3a). In contrast, a strong increase in Iba1 staining was detected in all LPS-injected mouse lines attesting the microglial activation (Fig. 3a,b and supplementary Fig. S4). Remarkably, endogenous fluorescence of P2X4mCherryIN was directly visible and colocalized with Iba1 in CMV mice, but not in Floxed or CaMK2 mice. Anti-RFP confirmed the abundant and specific P2X4mCherryIN expression in Iba1-positive cells solely in LPS-treated CMV mice. Notably, using Beno-271, a camelid nanobody recognizing the extracellular domain of mouse P2X4 [52], we showed increased P2X4 surface expression in microglia of CMV, CaMK2 and Floxed but not of P2X4KO mice (Fig. 3b and supplementary Fig. S4). These results validate the cellular specificity of the Cre-mediated excision in both knock-in mice and show that *de novo* expression of P2X4 induced by LPS can be directly monitored by the visualization of the fluorescence of mCherry fused to P2X4.

P2X4 has been shown to be highly expressed in macrophages[41]. Endogenous mCherry fluorescence was directly visualized in freshly isolated peritoneal macrophages from CMV mice (Fig. 3c), the only knock-in line expressing P2X4mCherryIN receptors in macrophages as confirmed by western blots of macrophages isolated from CMV, CaMK2, Floxed and P2X4KO mice (Fig. 3d). To assess surface/total ratio of P2X4 and P2X4mCherryIN by western blot analysis, biotinylation assays were performed using macrophages in suspension. Our results showed that the number of surface P2X4mCherryIN is

significantly higher in CMV (Fig. 3e,f) than in Floxed mice expressing P2X4WT, demonstrating that the substitution of P2X4 by P2X4mCherryIN leads to an increase in surface P2X4 density in macrophages from CMV mice.

**P2X4mCherryIN is differentially upregulated at the surface of neurons and glia in CMV and CaMK2 mice**

To demonstrate surface upregulation of P2X4mCherryIN in the CNS, we performed immunofluorescence experiments using hippocampal cultures from pups of both CMV, CaMK2 Floxed or P2X4KO mice. We showed the distribution of surface *versus* intracellular P2X4 using antibodies targeting either the native extracellular domain of P2X4 (Nodu-246), or against the intracellular C-tail of either P2X4WT (anti-P2X4) or P2X4mCherryIN (anti-RFP, Fig. 4). In the Floxed mice, most P2X4WT was detected intracellularly (Fig. 4a) as described previously[27, 28, 34]. In contrast, in both CMV and CaMK2 cells, a strong surface staining was detected using Nodu-246, as well as the presence of RFP labeling, indicating the high density of P2X4mCherryIN on the surface of these hippocampal cells (Fig. 4a). In cells from P2X4KO mice, no P2X4 was detected on the cell surface or intracellular (Fig. 4a). Anti-MAP2 antibodies revealed the specific expression of P2X4mCherryIN in neurons in both CMV and CaMK2 transgenic lines (Fig. 4b and supplementary Fig. S5a). Using antibodies against astrocytic GFAP and microglial Iba1 markers combined with Nodu-246 and anti-RFP, revealed the presence of surface P2X4mCherryIN in microglia and astrocytes from CMV, but not CaMK2 mice (Fig. 4c-d and supplementary Fig. S5b). Consistently, Western blotting of proteins extracted from hippocampal cultures of the different knock-in lines allowed the identification of P2X4mCherryIN proteins in the CMV and CaMK2 exclusively, whereas P2X4WT was detected in Floxed and CaMK2 hippocampal cells (Fig. 4e). Next, we examined surface and total P2X4 levels using either anti-P2X4 or anti-RFP antibodies by biotinylation assays and western blotting of hippocampal cells from the different transgenic mice. Quantification of immunoblots (Fig. 4f) clearly indicates that P2X4WT in Floxed and CaMK2 mice is mainly intracellular (Fig. 4g), while the amount of P2X4mCherryIN on the cell surface is significantly higher in both CMV and CaMK2 cells (Fig. 4a-d). Altogether, these results confirm that substitution of

P2X4WT by P2X4mCherryIN is restricted to excitatory neurons of CaMK2 mice while in CMV mice, the substitution occurs in all cells endogenously expressing P2X4 in CMV mice. In addition, our results demonstrate that P2X4mCherryIN expression leads to a stronger surface localization of P2X4mCherryIN in both CMV and CaMK2 mice (Fig. 4g).

**Increased surface density of P2X4 alters LTP and LTD at CA1 hippocampal synapses**

We next examined the impact of non-internalized P2X4mCherryIN in hippocampal synaptic plasticity. Field excitatory postsynaptic potential (fEPSP) were recorded in the hippocampal CA1 region after stimulation of presynaptic Schaffer collateral axons in acute brain slices from control Floxed and both CaMK2 or CMV mice (Fig. 5a-f). The input/output curves obtained by plotting fEPSP slopes against the amplitude of stimulation (Fig. 5b) showed no significant differences between slices from CMV or CaMK2 mice compared to control Floxed mice indicating that increased P2X4 surface receptors do not disrupt basal excitatory transmission at CA1 synapses. LTP and LTD were then evaluated. Robust LTP was induced in slices from Floxed mice with persistent potentiation (Fig. 5c,d). High frequency stimulation failed to trigger a potentiation in CaMK2 slices, while in CMV slices a potentiation was induced, but evoked responses returned rapidly to baseline after the induction. At 40 min post-induction, LTP was absent in slices from both CMV and CaMK2 mice (Fig. 5c,d). Increased surface P2X4 appears to block LTD as well (Fig. 5e,f). LTD was induced in slices from Floxed, CMV and CaMK2 mice but a significant persistent synaptic depression was recorded solely in Floxed mice only (Fig. 5e,f). LTD from CMV and CaMK2 slices was not significantly different from baseline. Altogether, these results demonstrate that increased surface P2X4 blocks LTP and alters LTD at hippocampal CA1 synapses. Moreover, the effects are more pronounced when surface P2X4 is increased exclusively in forebrain excitatory neurons.

**Increased surface density of P2X4 in forebrain neurons alters anxiety and memory functions**

Next, the impact of non-internalized P2X4mCherryIN expression on the behavior of the different transgenic mice was then examined using a battery of tests (Fig. 5g-p and Supplementary Fig. S6).

First, potential changes in their general activity were assessed during open field exploration (Fig. 5g-i). Floxed, CaMK2 and CMV mice showed similar velocity and total distance traveled in the arena, indicating that increased surface P2X4 does not modulate basal locomotor activity (Fig. 5g,h and Supplementary Fig. S6b). Interestingly, CaMK2 mice spent significantly more times in the central zone (red area) compared to the other groups of mice (Fig. 5i), suggesting that increased surface P2X4 density may reduce anxiety-like behavior. Neophobia-related anxiety was additionally examined by placing a novel object in the center of the arena (Fig. 5j-l; [56]). The latency to first exploring the novel object was slightly lower for CaMK2 than for CMV and Floxed mice but this difference failed to reach significance (Fig. 5k). However, CaMK2 mice spent significantly more time exploring the object than Floxed or CMV mice (Fig. 5l), suggesting that anxiety is lower in these mice. To corroborate these findings, the three mouse lines were tested in the elevated plus maze (Fig. 5m). Compared to CMV and Floxed mice, CaMK2 mice spent a greater proportion of time in the open arms of the maze, confirming their anxiolytic phenotype. These results indicate that neuronal P2X4 is involved in the regulation of anxiety-like behavior, with an increased number of P2X4 on neuronal surfaces resulting in reduced anxiety.

Spatial recognition memory was then evaluated using a modified version of the Y-maze two-trial arm discrimination task (Fig. 5n and Supplementary fig. S6; [57]). After a single encoding phase of 10 min with only two accessible arms, an inter-trial interval of 4 h resulted in a robust and similar preference for the unexplored, previously inaccessible, arm during the test phase in CMV, CaMK2 and Floxed mice. Thus, mice from all genotypes were capable of processing visuo-spatial information and forming short-term spatial recognition memory.

We next asked whether impairments in learning and memory underlie the observed synaptic plasticity deficits. We examined spatial memory in a more cognitively-challenging situation by submitting CMV, CaMK2 and Floxed mice to spatial discrimination tests in the 8-arm radial maze. Mice were required to locate the 3 constantly baited arms of the maze (Fig. 5o). To provide a rigorous control over the time course of neuronal events induced by spatial learning, we trained the mice over one single day. Reference memory training consisted of four equivalent blocks of six trials separated by a 1 h interval.

Each trial started with all 8 arms opened and terminated when the mouse entered the third baited arm and returned to the central platform of the maze. While the number of reference memory errors (i.e., entries into unbaited arms) decreased significantly over the four training blocks in all three mouse lines (Fig. 5o), CaMK2 mice made significantly more errors than CMV and Floxed mice (Fig. 5k, p= 0.0094). Poorer performance of CaMK2 was particularly apparent in training blocks 2 and 4 compared to Floxed and CMV mice. Subsequently recent and long-term memory were evaluated by by submitting mice to retrieval testing 1 and 14 days after training completion (Fig. 5p). As expected, Floxed mice exhibited memory decay over time with an increased number of reference memory errors at day 14. A similar decay was observed in CMV mice, indicating that forgetting was unaffected in this mouse line. In contrast, the poorer performance of CaMK2 mice achieved upon training remained stable across delays and was not further exacerbated by the passage of time. At Day 14, the number of reference memory errors was elevated but similar for all three genotypes. Thus, selective expression of non-internalized P2X4mCherryIN in excitatory forebrain neurons translated into impaired spatial memory processing.

## Discussion

To address pathologically increased surface P2X4 functions, we created a floxed knock-in P2X4mCherryIN mouse line and generated two distinct conditional P2X4mCherryIN lines, expressing non-internalized P2X4mCherryIN either in all cells natively expressing P2X4 (CMV mice) or in excitatory forebrain neurons (CaMK2 mice), respectively. Both CMV and CaMK2 P2X4mCherryIN knock-in mice were viable, reproduced normally and displayed no manifest phenotypic issues. The key finding of this study is that the increased surface density of P2X4 in forebrain excitatory neurons is a major regulator of hippocampal synaptic plasticity, learning and memory and anxiety functions indicating that increased neuronal P2X4 observed in AD models may have key role in the pathogenesis of AD[25].

Importantly, analysis of P2X4mCherryIN expression showed that substitution of P2X4WT by P2X4mCherryIN occurred in the expected brain regions in both strains. In CMV mice, the expression

pattern of P2X4mCherryIN is consistent with what was described for wild-type P2X4 in the CNS, *i.e*. high expression in the olfactory epithelium and a sparse expression in the hippocampus, cortex, cerebellum and spinal cord[3, 15, 53]. In addition, and in line with other findings[41, 58], P2X4mCherryIN was also found expressed in peritoneal macrophages of CMV mice. In CaMK2 mice, P2X4mCherryIN expression was mainly restricted to hippocampal and cortical regions, in line with previous reports of CaMK2 promoter selectivity [59]. The *in vitro* expression of P2X4mCherryIN construct revealed that the substitution of the last 11 amino acids of the C-tail of mouse P2X4 by the red fluorescent protein mCherry increases surface trafficking without altering P2X4 function and subcellular targeting[3, 27, 28, 30, 42, 43]. Indeed, in both CMV and CaMK2 knock-in mice, electron microscopy confirmed that P2X4mCherryIN are localized at both pre- and post-synaptic specializations in hippocampal or cortical excitatory neurons, as expected[2, 3, 15]. Inhibitory symmetric synapses are difficult to identify based on morphology criteria, thus the presence of P2X4mCherryIN at the GABAergic synapse, where P2X4 was reported to be present, remains to be shown by including specific markers[9, 10, 42]. Surface and intracellular staining on hippocampal cultures as well as biotinylation experiments from the different knock-in mice demonstrate that substitution of P2X4WT by P2X4mCherryIN induced a significant increase in surface P2X4 in both CaMK2 and CMV neurons. Additionally, P2X4mCherryIN was found to be present and upregulated at the surface of hippocampal microglia and astrocytes as well as macrophages of CMV mice. P2X4 expression in astrocytes has been previously observed, but was debated[60]. Notably, P2X4mCherryIN was detected in hippocampal astrocytes *in vitro*, but was detected on brain slices by E.M. only.

In contrast to transfected cells over-expressing P2X4mCherryIN, direct fluorescence of P2X4mCherryIN was undetectable from brain slices and hippocampal cultures of both knock-in mice, preventing the direct identification and functional characterization of P2X4mCherryIN-expressing cells. Fluorescence of P2X4mCherryIN was directly visible solely in isolated peritoneal macrophages of CMV mice in agreement with its high basal expression in macrophages[41]. Interestingly, following LPS injection in the hippocampus to induce microglial activation and increase *de novo* P2X4 expression[15], endogenous fluorescence of P2X4mCherryIN was revealed in Iba1-positive microglia exclusively in CMV mice.

These results indicate that the P2X4mCherryIN fluorescence may represent a unique tool to directly monitor increased P2X4 expression in pathological models such as chronic pain, AD, ALS, alcohol intake, inflammation, epilepsy, ischemia or brain trauma [14, 19, 22, 23, 25, 26, 35-38, 55, 61].

LTP and LTD phenomena are widely recognized as crucial molecular mechanisms underlying cognitive functions such as learning and memory[62]. Although activation of P2X receptors by glial ATP was recently shown to directly modulate glutamatergic synaptic strength[10], P2X receptors exert modulatory actions exclusively during activity-dependent plasticity at central synapses and do not influence basal synaptic transmission [17, 18, 63]. Previous studies have shown P2X4 modulating hippocampal LTP via N-methyl-D-aspartate receptor receptors (NMDAR), however these findings remained controversial. The first work using P2X4KO mice revealed that LTP in CA1 neurons was slightly reduced compared to wild-type mice and that potentiation of P2X4 by ivermectin enhanced LTP only in wild-type mice[17]. Results suggested that P2X4 may enhance the content of NR2B subunits in synaptic NMDARs[63]. In contrast, an other study showed that the pharmacological blockade of P2X4 facilitated the induction of NMDAR-dependent LTP indicating an inhibitory impact of P2X4[18, 64]. Furthermore , increased P2X4 expression was reported in AD models[25] suggesting that P2X4 might also contribute to synaptic dysfunction and memory deficits. Field potential recordings show that P2X4mCherryIN expression does not change the basal excitatory transmission at CA1 synapses but causes impairments in both LTP and LTD in agreement with a negative impact of P2X4 on synaptic plasticity. Surprisingly, but in full agreement with our behavioral results, these deficits were stronger in CaMK2 than in CMV mice. Impaired LTP observed in CaMK2 mice occurred immediately suggesting a deficit of LTP induction. In contrast, in CMV mice, LTP was induced but progressively returned to baseline, rather indicating a deficit in LTP maintenance. Since basal excitation mediated by α-amino-3-hydroxy-5-methyl-4-isoxazolepropionic acid receptor (AMPAR) is unchanged, and LTD or LTP in hippocampal CA1 neurons are mainly initiated post-synaptically by NMDAR[62], our results suggest that increased P2X4 in CA1 neurons might alter NMDAR function. P2X4 are highly permeable to calcium and can mediate a strong calcium influx at the resting membrane potential that may induce NMDAR inactivation[64]. P2X4 interacts also dynamically with

various other ligand-gated ion channels such as $GABA_A$[10, 42, 65] and may lead to NMDAR inhibition by similar crosstalk.

Behavioral phenotyping of the CMV mice did not reveal any overt alterations. In contrast, CaMK2 mice exhibited a significant decrease in anxiety-like behaviors and impaired spatial learning and memory functions. No change in locomotor, anxiety-like or cognitive functions were previously observed in P2X4KO mice [66]. Together, these results suggest that, in contrast to the basal state, increased surface P2X4 density observed in neurons in pathological situations such as in AD [25] might play essential roles in the regulation of synaptic plasticity and behavior such as anxiety and learning and memory.

The absence of a phenotype of the CMV mice, although in agreement with the weaker effects on the synaptic plasticity of CMV compared to CaMK2 mice, is intriguing since substitution of P2X4WT by P2X4mCherryIN in all cells natively expressing P2X4 was expected to have more pronounced effects than specific P2X4mCherryIN expression solely in forebrain excitatory neurons. However, this could be explained by temporal differences between CMV and CaMK2 promoter activation. CMV is a ubiquitous early-gene promoter leading to the genetic excision of Floxed P2X4mCherryIN in the germ-line and consequently from the beginning of the embryonic development while the CaMK2 promoter is considered as an adult promoter with postnatal activity reaching its maximum around the third postnatal week [67]. Expression of P2X4mCherryIN in all cells natively expressing P2X4 during the developmental period and thereafter may have deleterious effects leading to developmental compensations. Another possibility is that the expression of P2X4mCherryIN in CMV mice in other types of neurons along with expression in glial cells may counterbalance the effect of its increased surface density specifically in excitatory neurons. Indeed, increased P2X4 expression in spinal cord microglia during neuropathic conditions triggers the release of BDNF by microglia resulting in neuronal hyperexcitability [39, 40]. In addition, microglia and BDNF have been shown to influence synaptic plasticity and learning in the brain [68]. These results suggest that increased surface P2X4 in microglia of CMV mice may promote synaptic plasticity and counterbalance the negative impact of an increase of surface P2X4 specifically in excitatory neurons of CaMK2 mice.

P2X4 is present in multiple cell types in the peripheral or central nervous system and in various epithelial, endothelial or immune cells. After injury and during inflammation and cell damage, high levels of ATP are released and P2X4 are strongly upregulated on cell surfaces. This upregulation seems to orchestrate key events during neurodegenerative diseases, neuropathic and inflammatory pain, ischemia-induced inflammation, alcohol intake, airways inflammation in asthma, rheumatoid arthritis or postsurgical liver regeneration (see for review[14]).

These novel conditional knock-in mice defective for P2X4 internalization provide a valuable tool which will allow to further decipher the role of upregulated P2X4 state not only in the context of neurological diseases, but also of peripheral inflammation, infection as well as in lung, cardiac or liver functions [69-73].


## Acknowledgements

We thank G. Dabee for the production of all transgenic mice at the animal facility, H. Orignac for help with *Xenopus* facilities and E. Normand for stereotaxic injection. We thank the Mouse Clinical Institute (Institut Clinique de la Souris, MCI/ICS) in the Genetic Engineering and Model Validation Department who established the mouse mutant floxed P2X4mCherryIN line. We also thank the biochemistry facility of Bordeaux Neurocampus. Electron microscopy was performed at the Bordeaux Imaging Center, a service unit of the CNRS-INSERM and Bordeaux University. This work was supported by CNRS, University of Bordeaux, a grant LabEx BRAIN ANR-10-LABX-43 to EB-G and EB, a grant from Inserm for the generation of the mouse line to EB-G, the Louise and Alan Edwards Foundation, an awarded grant from Quebec Pain Research Network (QPRN) to TD, International Ph. D program of the IdEx of Bordeaux to EB-G and PS and DFG grant SFB1328-Z02 to FK-N.


## Author contributions

EB, TD, KSP, AM, J-TP, ED, A-EA, ET, MR, FG, ON performed the experiments and analyzed the data. PS, BB, SL, FG, SB, ON and EB-G designed the experiments and analyzed the data. PB, EB, FK-N

contributed with key reagents. EB-G conceived the knock-in mice and the study. KSP, ON, and EB-G wrote the manuscript. All authors commented the manuscript.

## Conflict of interest

The authors declare they have no conflict of interest.

## Supplementary information is available at MP's website

## References


1. Khakh BS, North RA. Neuromodulation by extracellular ATP and P2X receptors in the CNS. *Neuron* 2012; **76**(1)**:** 51-69.

2. Rodrigues RJ, Almeida T, Richardson PJ, Oliveira CR, Cunha RA. Dual presynaptic control by ATP of glutamate release via facilitatory P2X1, P2X2/3, and P2X3 and inhibitory P2Y1, P2Y2, and/or P2Y4 receptors in the rat hippocampus. *J Neurosci* 2005; **25**(27)**:** 6286-6295.

3. Rubio ME, Soto F. Distinct Localization of P2X receptors at excitatory postsynaptic specializations. *J Neurosci* 2001; **21**(2)**:** 641-653.

4. Kaczmarek-Hajek K, Zhang J, Kopp R, Grosche A, Rissiek B, Saul A *et al.* Re-evaluation of neuronal P2X7 expression using novel mouse models and a P2X7-specific nanobody. *Elife* 2018; **7**.

5. Jo YH, Schlichter R. Synaptic corelease of ATP and GABA in cultured spinal neurons. *Nat Neurosci* 1999; **2**(3)**:** 241-245.

6. Mori M, Heuss C, Gahwiler BH, Gerber U. Fast synaptic transmission mediated by P2X receptors in CA3 pyramidal cells of rat hippocampal slice cultures. *J Physiol* 2001; **535**(Pt 1)**:** 115-123.

7. Gordon GR, Baimoukhametova DV, Hewitt SA, Rajapaksha WR, Fisher TE, Bains JS. Norepinephrine triggers release of glial ATP to increase postsynaptic efficacy. *Nat Neurosci* 2005; **8**(8)**:** 1078-1086.

8. Pougnet JT, Toulme E, Martinez A, Choquet D, Hosy E, Boue-Grabot E. ATP P2X receptors downregulate AMPA receptor trafficking and postsynaptic efficacy in hippocampal neurons. *Neuron* 2014; **83**(2)**:** 417-430.

9. Lalo U, Palygin O, Rasooli-Nejad S, Andrew J, Haydon PG, Pankratov Y. Exocytosis of ATP from astrocytes modulates phasic and tonic inhibition in the neocortex. *PLoS Biol* 2014; **12**(1)**:** e1001747.

10. Boué-Grabot E, Pankratov Y. Modulation of Central Synapses by Astrocyte-Released ATP and Postsynaptic P2X Receptors. *Neural Plast.*, vol. 20172017, p 9454275.

11. Illes P, Verkhratsky A. Purinergic neurone-glia signalling in cognitive-related pathologies. *Neuropharmacology* 2016; **104:** 62-75.

12. Kawate T, Michel JC, Birdsong WT, Gouaux E. Crystal structure of the ATP-gated P2X(4) ion channel in the closed state. *Nature* 2009; **460**(7255)**:** 592-598.

13. Egan TM, Khakh BS. Contribution of calcium ions to P2X channel responses. *J Neurosci* 2004; **24**(13)**:** 3413-3420.

14. Suurväli J, Boudinot P, Kanellopoulos J, Rüütel Boudinot S. P2X4: A fast and sensitive purinergic receptor. *Biomedical Journal*, vol. 40. Elsevier2017, pp 245-256.

15. Xu J, Bernstein AM, Wong A, Lu XH, Khoja S, Yang XW *et al.* P2X4 Receptor Reporter Mice: Sparse Brain Expression and Feeding-Related Presynaptic Facilitation in the Arcuate Nucleus. *J Neurosci* 2016; **36**(34)**:** 8902-8920.

16. Yeung D, Kharidia R, Brown SC, Gorecki DC. Enhanced expression of the P2X4 receptor in Duchenne muscular dystrophy correlates with macrophage invasion. *Neurobiol Dis* 2004; **15**(2)**:** 212-220.

17. Sim JA, Chaumont S, Jo J, Ulmann L, Young MT, Cho K *et al.* Altered hippocampal synaptic potentiation in P2X4 knock-out mice. *J Neurosci* 2006; **26**(35)**:** 9006-9009.

18. Pankratov Y, Lalo U, Krishtal OA, Verkhratsky A. P2X receptors and synaptic plasticity. *Neuroscience* 2008.

19. Cavaliere F, Florenzano F, Amadio S, Fusco FR, Viscomi MT, D'Ambrosi N *et al.* Up-regulation of P2X2, P2X4 receptor and ischemic cell death: prevention by P2 antagonists. *Neuroscience* 2003; **120**(1)**:** 85-98.

20. Franke H, Illes P. Involvement of P2 receptors in the growth and survival of neurons in the CNS. *Pharmacol Ther* 2006; **109**(3)**:** 297-324.

21. Burnstock G. Purinergic signalling and disorders of the central nervous system. *Nat Rev Drug Discov* 2008; **7**(7)**:** 575-590.

22. Apolloni S, Montilli C, Finocchi P, Amadio S. Membrane compartments and purinergic signalling: P2X receptors in neurodegenerative and neuroinflammatory events. *Febs J* 2009; **276**(2)**:** 354-364.

23. Volonte C, Apolloni S, Parisi C, Amadio S. Purinergic contribution to amyotrophic lateral sclerosis. *Neuropharmacology* 2016; **104:** 180-193.

24. Beggs S, Trang T, Salter MW. P2X4R+ microglia drive neuropathic pain. *Nat Neurosci* 2012; **15**(8)**:** 1068-1073.

25. Varma R, Chai Y, Troncoso J, Gu J, Xing H, Stojilkovic SS *et al.* Amyloid-beta induces a caspase-mediated cleavage of P2X4 to promote purinotoxicity. *Neuromolecular Med* 2009; **11**(2)**:** 63-75.

26. Casanovas A, Hernandez S, Tarabal O, Rossello J, Esquerda JE. Strong P2X4 purinergic receptor-like immunoreactivity is selectively associated with degenerating neurons in transgenic rodent models of amyotrophic lateral sclerosis. *J Comp Neurol* 2008; **506**(1)**:** 75-92.

27. Bobanovic LK, Royle SJ, Murrell-Lagnado RD. P2X receptor trafficking in neurons is subunit specific. *J Neurosci* 2002; **22**(12)**:** 4814-4824.

28. Royle SJ, Bobanovic LK, Murrell-Lagnado RD. Identification of a non-canonical tyrosine-based endocytic motif in an ionotropic receptor. *J Biol Chem* 2002; **277**(38)**:** 35378-35385.

29. Qureshi OS, Paramasivam A, Yu JC, Murrell-Lagnado RD. Regulation of P2X4 receptors by lysosomal targeting, glycan protection and exocytosis. *J Cell Sci* 2007; **120**(Pt 21)**:** 3838-3849.

30. Royle SJ, Qureshi OS, Bobanovic LK, Evans PR, Owen DJ, Murrell-Lagnado RD. Non-canonical YXXGPhi endocytic motifs: recognition by AP2 and preferential utilization in P2X4 receptors. *J Cell Sci* 2005; **118**(Pt 14)**:** 3073-3080.

31. Toulme E, Garcia A, Samways D, Egan TM, Carson MJ, Khakh BS. P2X4 receptors in activated C8-B4 cells of cerebellar microglial origin. *J Gen Physiol* 2010; **135**(4)**:** 333-353.

32. Cao Q, Zhong XZ, Zou Y, Murrell-Lagnado R, Zhu MX, Dong XP. Calcium release through P2X4 activates calmodulin to promote endolysosomal membrane fusion. *J Cell Biol* 2015; **209**(6)**:** 879-894.

33. Huang P, Zou Y, Zhong XZ, Cao Q, Zhao K, Zhu MX *et al.* P2X4 forms functional ATP-activated cation channels on lysosomal membranes regulated by luminal pH. *J Biol Chem* 2014; **289**(25)**:** 17658-17667.

34. Robinson LE, Murrell-Lagnado RD. The trafficking and targeting of P2X receptors. *Front Cell Neurosci* 2013; **7:** 233.

35. Andries M, Van Damme P, Robberecht W, Van Den Bosch L. Ivermectin inhibits AMPA receptor-mediated excitotoxicity in cultured motor neurons and extends the life span of a transgenic mouse model of amyotrophic lateral sclerosis. *Neurobiol Dis* 2007; **25**(1)**:** 8-16.

36. Khoja S, Huynh N, Asatryan L, Jakowec MW, Davies DL. Reduced expression of purinergic P2X4 receptors increases voluntary ethanol intake in C57BL/6J mice. *Alcohol* 2018; **68:** 63-70.

37. Wyatt LR, Finn DA, Khoja S, Yardley MM, Asatryan L, Alkana RL *et al.* Contribution of P2X4 receptors to ethanol intake in male C57BL/6 mice. *Neurochemical research* 2014; **39**(6)**:** 1127-1139.

38. Tsuda M, Shigemoto-Mogami Y, Koizumi S, Mizokoshi A, Kohsaka S, Salter MW *et al.* P2X4 receptors induced in spinal microglia gate tactile allodynia after nerve injury. *Nature*, vol. 4242003, pp 778-783.

39. Ulmann L, Hatcher JP, Hughes JP, Chaumont S, Green PJ, Conquet F *et al.* Up-regulation of P2X4 receptors in spinal microglia after peripheral nerve injury mediates BDNF release and neuropathic pain. *J Neurosci* 2008; **28**(44)**:** 11263-11268.

40. Coull JA, Beggs S, Boudreau D, Boivin D, Tsuda M, Inoue K *et al.* BDNF from microglia causes the shift in neuronal anion gradient underlying neuropathic pain. *Nature* 2005; **438**(7070)**:** 1017-1021.

41. Ulmann L, Hirbec H, Rassendren F. P2X4 receptors mediate PGE2 release by tissue-resident macrophages and initiate inflammatory pain. *EMBO J*, vol. 292010, pp 2290-2300.

42. Jo YH, Donier E, Martinez A, Garret M, Toulme E, Boue-Grabot E. Cross-talk between P2X4 and gamma-aminobutyric acid, type A receptors determines synaptic efficacy at a central synapse. *J Biol Chem* 2011; **286**(22)**:** 19993-20004.

43. Toulme E, Soto F, Garret M, Boue-Grabot E. Functional properties of internalization-deficient P2X4 receptors reveal a novel mechanism of ligand-gated channel facilitation by ivermectin. *Mol Pharmacol* 2006; **69**(2)**:** 576-587.

44. Chamma I, Heubl M, Chevy Q, Renner M, Moutkine I, Eugene E *et al.* Activity-dependent regulation of the K/Cl transporter KCC2 membrane diffusion, clustering, and function in hippocampal neurons. *J Neurosci* 2013; **33**(39)**:** 15488-15503.

45. Ray A, Dittel BN. Isolation of mouse peritoneal cavity cells. *Journal of visualized experiments : JoVE* 2010; (35).

46. Berthet A, Porras G, Doudnikoff E, Stark H, Cador M, Bezard E *et al.* Pharmacological analysis demonstrates dramatic alteration of D1 dopamine receptor neuronal distribution in the rat analog of L-DOPA-induced dyskinesia. *J Neurosci* 2009; **29**(15)**:** 4829-4835.

47. Bertin E, Martinez A, Boue-Grabot E. P2X Electrophysiology and Surface Trafficking in Xenopus Oocytes. *Methods Mol Biol* 2020; **2041:** 243-259.

48. Belzung C. Hippocampal mossy fibres: implication in novelty reactions or in anxiety behaviours? *Behav Brain Res* 1992; **51**(2)**:** 149-155.

49. Renner MJ, Bennett AJ, White JC. Age and sex as factors influencing spontaneous exploration and object investigation by preadult rats (Rattus norvegicus). *J Comp Psychol* 1992; **106**(3)**:** 217-227.

50. Pellow S, File SE. Anxiolytic and anxiogenic drug effects on exploratory activity in an elevated plus-maze: a novel test of anxiety in the rat. *Pharmacol Biochem Behav* 1986; **24**(3)**:** 525-529.

51. Dellu F, Contarino A, Simon H, Koob GF, Gold LH. Genetic differences in response to novelty and spatial memory using a two-trial recognition task in mice. *Neurobiol Learn Mem* 2000; **73**(1)**:** 31-48.

52. Bergmann P, Garcia de Paco A, Rissiek B, Menzel S, Dubberke G, Hua J *et al.* Generation and characterization of specific monoclonal antibodies and Nanobodies directed against the ATP-gated channel P2X4. *Frontiers in Cellular Neuroscience* in press.

53. Lê KT, Villeneuve P, Ramjaun AR, McPherson PS, Beaudet A, Seguela P. Sensory presynaptic and widespread somatodendritic immunolocalization of central ionotropic P2X ATP receptors. *Neuroscience*, vol. 831998, pp 177-190.

54. Buell G, Lewis C, Collo G, North RA, Surprenant A. An antagonist-insensitive P2X receptor expressed in epithelia and brain. *The EMBO journal* 1996; **15**(1)**:** 55-62.

55. Ulmann L, Levavasseur F, Avignone E, Peyroutou R, Hirbec H, Audinat E *et al.* Involvement of P2X4 receptors in hippocampal microglial activation after status epilepticus. *Glia* 2013; **61**(8)**:** 1306-1319.

56. Dulawa SC, Grandy DK, Low MJ, Paulus MP, Geyer MA. Dopamine D4 receptor-knock-out mice exhibit reduced exploration of novel stimuli. *J Neurosci* 1999; **19**(21)**:** 9550-9556.

57. Nicole O, Hadzibegovic S, Gajda J, Bontempi B, Bem T, Meyrand P. Soluble amyloid beta oligomers block the learning-induced increase in hippocampal sharp wave-ripple rate and impair spatial memory formation. *Sci Rep* 2016; **6:** 22728.

58. Layhadi JA, Turner J, Crossman D, Fountain SJ. ATP Evokes Ca(2+) Responses and CXCL5 Secretion via P2X4 Receptor Activation in Human Monocyte-Derived Macrophages. *J Immunol* 2018; **200**(3)**:** 1159-1168.

59. Tsien JZ, Chen DF, Gerber D, Tom C, Mercer EH, Anderson DJ *et al.* Subregion- and cell type-restricted gene knockout in mouse brain. *Cell* 1996; **87**(7)**:** 1317-1326.

60. Stokes L, Layhadi JA, Bibic L, Dhuna K, Fountain SJ. P2X4 Receptor Function in the Nervous System and Current Breakthroughs in Pharmacology. *Front Pharmacol* 2017; **8:** 291.

61. Franklin KM, Asatryan L, Jakowec MW, Trudell JR, Bell RL, Davies DL. P2X4 receptors (P2X4Rs) represent a novel target for the development of drugs to prevent and/or treat alcohol use disorders. *Front Neurosci* 2014; **8:** 176.

62. Huganir RL, Nicoll RA. AMPARs and synaptic plasticity: the last 25 years. *Neuron* 2013; **80**(3)**:** 704-717.

63. Baxter AW, Choi SJ, Sim JA, North RA. Role of P2X4 receptors in synaptic strengthening in mouse CA1 hippocampal neurons. *Eur J Neurosci* 2011; **34**(2)**:** 213-220.

64. Pankratov YV, Lalo UV, Krishtal OA. Role for P2X receptors in long-term potentiation. *J Neurosci* 2002; **22**(19)**:** 8363-8369.

65. Jo YH, Boue-Grabot E. Interplay between ionotropic receptors modulates inhibitory synaptic strength. *Commun Integr Biol* 2011; **4**(6)**:** 706-709.

66. Wyatt LR, Godar SC, Khoja S, Jakowec MW, Alkana RL, Bortolato M *et al.* Sociocommunicative and Sensorimotor Impairments in Male P2X4-Deficient Mice. *Neuropsychopharmacology*, vol. 38. Nature Publishing Group2013, pp 1993-2002.

67. Mayford M, Bach ME, Huang YY, Wang L, Hawkins RD, Kandel ER. Control of memory formation through regulated expression of a CaMKII transgene. *Science* 1996; **274**(5293)**:** 1678-1683.

68. Parkhurst CN, Yang G, Ninan I, Savas JN, Yates JR, 3rd, Lafaille JJ *et al.* Microglia promote learning-dependent synapse formation through brain-derived neurotrophic factor. *Cell* 2013; **155**(7)**:** 1596-1609.

69. Hafner S, Wagner K, Weber S, Groger M, Wepler M, McCook O *et al.* Role of the Purinergic Receptor P2XR4 After Blunt Chest Trauma in Cigarette Smoke-Exposed Mice. *Shock* 2017; **47**(2)**:** 193-199.

70. Chen H, Xia Q, Feng X, Cao F, Yu H, Song Y *et al.* Effect of P2X4R on airway inflammation and airway remodeling in allergic airway challenge in mice. *Mol Med Rep* 2016; **13**(1)**:** 697-704.

71. Yang T, Shen JB, Yang R, Redden J, Dodge-Kafka K, Grady J *et al.* Novel protective role of endogenous cardiac myocyte P2X4 receptors in heart failure. *Circ Heart Fail* 2014; **7**(3)**:** 510-518.

72. Pettengill MA, Marques-da-Silva C, Avila ML, d'Arc dos Santos Oliveira S, Lam VW, Ollawa I *et al.* Reversible inhibition of Chlamydia trachomatis infection in epithelial cells due to stimulation of P2X(4) receptors. *Infect Immun* 2012; **80**(12)**:** 4232-4238.

73. Gonzales E, Julien B, Serriere-Lanneau V, Nicou A, Doignon I, Lagoudakis L *et al.* ATP release after partial hepatectomy regulates liver regeneration in the rat. *J Hepatol* 2010; **52**(1)**:** 54-62.

## Figure legends

**Fig. 1** Substitution of the internalization motif of P2X4 by mCherry increases ATP current density and surface expression of P2X4 receptors. **a** Schematic representation of the mouse P2X4 subunit topology and C-terminal sequence of wild-type P2X4 (WT) and P2X4mCherryIN subunits. The AP2 binding site (blue circle) within the C-terminal sequence of mouse P2X4WT was exchanged for the red fluorescent protein mCherry sequence (P2X4) preventing clathrin-dependent internalization. **b** Representative superimposed currents evoked by applications of ATP (100 µM, 5 s) from oocytes expressing wild-type P2X4 (WT) (black traces) or P2X4mCherryIN receptors (red traces). Bar graphs of the mean amplitude of ATP current recorded from oocytes expressing P2X4WT or P2X4mCherryIN as a function of the quantity of injected cDNAs. Recordings were performed the same day (2 or 3 days) post nuclear injection. Error bars represent s.e.m., number of cells is indicated in parentheses, $^{**}p < 0.01$, $^{***}p < 0.001$, one-way ANOVA and Tuckey's post hoc test. Blockade of P2X4 internalization induced a ~7-fold increase in ATP current amplitudes. **c** Specific detection by Western blots of total proteins from oocytes expressing P2X4WT (70 kDa) or P2X4mCherryIN (100 kDa) with anti-P2X4 or anti-RFP antibodies, respectively. **d** Representative immunoblots of total and surface biotinylated proteins from oocytes expressing P2X4WT (WT) or P2X4mCherryIN (mCherryIN) using anti-P2X4 or anti-RFP antibodies. Bars represent mean ± s.e.m. of the surface/total ratio of P2X4WT (grey bars, 4.73 ± 1.64%, n = 5) and P2X4mCherryIN (red bars, 27.05 ± 6.2%, n = 3). The number of independent experiments is indicated in parentheses, $^{*}p < 0.05$, unpaired t-test. **e** Confocal overlay images of hippocampal neurons transfected with extracellular HA-tagged P2X4WT or HA-P2X4mCherryIN revealed a strong increase in surface P2X4 in neurons expressing P2X4mCherryIN *vs* P2X4 WT. Surface P2X4 was revealed by labeling living cells with anti-HA antibodies (green). Total P2X4 was detected after fixation, permeabilization and staining with anti-P2X4 antibody (red) in P2X4 WT cells or by mCherry fluorescence (red) in P2X4mCherryIN cells. Scale bars, 20 µm. **f** Mean fluorescence intensity of surface HA-P2X4WT and HA-P2X4mCherryIN illustrated in E and in supplementary Fig. S1. Error bars, s.e.m., number of cells is indicated in parentheses, $^{***}p < 0.001$, unpaired Mann-Whitney test. **g,h** Enlarged

image of a dendrite, showing surface clustering of HA-P2X4mCherryIN. Postsynaptic regions are indicated by detection of Homer 1c (blue). Scale bar, 5 µm. 42% of clusters are localized in the vicinity of excitatory glutamatergic synapses. **g** Quantification of the size, fluorescence intensity and density of clusters at extrasynaptic site and in the vicinity of glutamatergic synapses showing P2X4 form larger clusters near synapses. Error bars: s.e.m., two-way ANOVA and Tuckey's post hoc test, interaction $F(2, 341) = 11.38$; ***$p < 0.001$. **i** Epifluorescence images of hippocampal neurons transfected with P2X4WT or P2X4mCherryIN revealed the strong increase of surface P2X4mCherryIN compared to P2X4WT. Surface P2X4WT and P2X4mCherryIN were revealed on living cells with Nodu-246 antibody (green) recognizing the native extracellular domain of P2X4. Total P2X4WT or P2X4mCherryIN were detected after fixation and permeabilization with anti-P2X4 antibodies (red) or directly by the red fluorescence of mCherry protein, respectively. Scale bar, 10 µm.

**Fig. 2** Generation of conditional P2X4mCherryIN knock-in mice and P2X4 expression in CMV-Cre or CaMK2-Cre P2X4mCherryIN knock-in mice. **a** Schematic diagram of the mouse *P2xr4* gene and targeting vector strategy used to generate floxed P2X4mCherryIN knock-in mice by homologous recombination (Floxed). By breeding floxed P2X4mCherryIN with CMV-Cre mice or CaMK2-Cre mice, we generated constitutive CMVCre-P2X4mCherryIN (CMV) and CaMK2Cre-P2X4mCherryIN (CaMK2) to obtain a gain-of-function of P2X4 in all cells or in excitatory forebrain neurons natively expressing P2X4, respectively. **b** Southern blot of genomic DNA of WT and targeted allele (Floxed) using external probe (P) after digestion by *Mfe I* or *Ssp I* enzyme (E) indicated in **a**. **c** Expression of P2X4WT and P2X4mCherryIN mRNAs by RT-PCR in cortex (Cx), cerebellum (Cb) and hippocampus (Hip) brain regions from Floxed P2X4mCherryIN, $CMVCre^{+}$/Floxed P2X4mCherryIN (CMV) and $CaMK2Cre^{+}$/Floxed P2X4mCherryIN (CaMK2) mice. **d-f** Protein expression of P2X4mCherryIN in the mouse brain revealed using anti-RFP antibodies recognizing mCherry protein. **d** Brain sections immunostained with anti-RFP antibodies show P2X4mCherryIN expression in the hippocampus and cortex of CMVCre-P2X4mCherryIN and CaMK2Cre-P2X4mCherryIN while no signal is visible in Floxed P2X4mCherryIN and P2X4 Knockout (KO) mice (see also supplementary Fig. S3). Scale bar, 20 µm. **e**

Western blotting of total proteins extracted from distinct CNS regions isolated from CMV-P2X4mCherryIN (CMV), CaMK2-P2X4mCherryIN (CaMK2), Floxed P2X4mCherryIN and P2X4KO mice revealed with anti-RFP or anti-P2X4 antibodies. Anti-Tubulin antibody was used as a loading control. OB, olfactory bulb; Hip, hippocampus; Cx, cortex; Cb, cerebellum; Hypo, hypothalamus; SC, spinal cord. **f** Electron microscopy images showing pre-embedding anti-RFP immunostaining in CA1 region of the hippocampus or cortex from CMV-P2X4mCherryIN and CaMK2-P2X4mCherryIN mice (see also supplementary Fig. S3). Staining is close to the plasma membrane of pre- and post-synaptic specializations of excitatory asymmetric synapses (top). Examples of spines where P2X4mCherryIN is detected only at the postsynapse, mainly located at the edge of the postsynaptic density. t, presynaptic; sp, spine. Scale bar, 0.5 µm.

**Fig. 3** Endogenous P2X4mCherryIN fluorescence in hippocampal microglia after LPS-induced de novo P2X4 expression and in peritoneal macrophages from CMV-P2X4mCherryIN mice. **a** Representative immunohistochemistry images of Iba1 and endogenous fluorescence of P2X4 mCherryIN (top, left) from the hippocampal region of the different mice injected with saline or 4 µg LPS on each side (see also supplementary Fig. S4). The mCherry fluorescence increased in Iba1-positive cells after LPS specifically in CMV mice. **b** Immunodetection of P2X4mCherryIN using Beno-271 antibodies (a Camelid nanobody directed against the extracellular domain of native P2X4) and anti-RFP antibodies from CMV or CaMK2 mice after LPS injections. An enlarged overlay reveals that the increase of P2X4mCherryIN is detected in Iba1-positive microglia cells by both antibodies in CMV mice while such increase is observed only with Beno-271 in CaMK2 mice. Scale Bar, 50 µm. **c** Endogenous P2X4mCherryIN fluorescence of macrophages isolated from the peritoneal cavity of Floxed and CMV mice. Differential interference contrast (DIC) and red fluorescence images reveal the P2X4mCherryIN exclusively in CMV mice. Scale bar, 20 µm. **d** Western blotting of total proteins from macrophages of CMV, CaMK2, Floxed and P2X4KO mice using anti-RFP and anti-P2X4 revealed that P2X4WT is substituted by P2X4mCherryIN in macrophages of CMV mice only. P2X4mCherryIN is not detected by anti-P2X4 directed against the C-terminal of P2X4. Anti-actin antibody was used as loading control. **e,f** Surface P2X4 expression is

increased in CMV mouse peritoneal macrophages. Representative immunoblots of total and biotinylated surface proteins from peritoneal macrophages isolated from Floxed and CMV mice revealed with anti-P2X4 and anti-RFP antibodies, respectively. As in **d**, total proteins of P2X4KO macrophages were used as a negative control. **f** Quantification of surface/total expression of P2X4WT and P2X4mCherryIN in macrophages shown representatively in **e**. Bars represent mean ± s.e.m. of the surface/total ratio of P2X4WT (Grey bar, 17.36 ± 1.03%, n = 53) in floxed mice and P2X4mCherryIN in CMV mice (red bar, 50.79 ± 2.71%, n = 51) and show that P2X4 surface expression is strongly increased in cells expressing P2X4mCherryIN mice compared to those expressing P2X4WT. The number of independent experiments is indicated by clear and black circles. *** $P < 0.001$, unpaired t-test.

**Fig. 4** Surface P2X4mCherryIN expression is increased in hippocampal neurons of CaMK2 or CMV mice as well as in glial cells of CMV mice. **a** Representative images of surface and total P2X4WT and/or P2X4mCherryIN in Floxed, CMV and CaMK2 primary hippocampal cell cultures reveal that surface P2X4mCherryIN is strongly increased compared to P2X4WT. Extracellular surface P2X4 and P2X4mCherryIN are visualized using Nodu-246 (green) antibodies. Intracellular P2X4WT is revealed by anti-P2X4 antibodies (red) in Floxed and P2X4KO mice while intracellular P2X4mCherryIN is revealed using anti-RFP antibodies (red) from CaMK2 and CMV mice. Staining was performed at 21 *div.* Scale bars, 10 µm. **b** High density of surface P2X4mCherryIN using Nodu-246 (green) is detected in CaMK2 and CMV neurons identified using neuronal MAP2 marker (magenta). Surface P2X4WT is almost absent in floxed mice and not detected in P2X4KO neurons (see supplementary Fig. S5). **c,d** P2X4mCherryIN is expressed only in astrocytes and microglia of CMV mice solely. **c** Surface and total P2X4mCherryIN revealed using Nodu-246 and anti-RFP antibodies (red) respectively, in GFAP-positive astrocytes (green) from 7 *div* primary hippocampal CMV cells. Nuclear marker DAPI is shown in blue. **d** Surface and total P2X4mCherryIN using Nodu-246 or anti-RFP antibodies (red), respectively, in microglia stained using anti-Iba1 antibodies (green) from 21 *div* primary hippocampal cells from CMV mice. Nuclear marker DAPI is shown in blue. **e** Western blotting of total proteins from primary hippocampal cells from Floxed, CMV, CaMK2, and P2X4KO mice using anti-RFP and anti-P2X4 antibodies reveal

P2X4mCherryIN specifically in CMV and CaMK2 mice while P2X4WT is detected in CaMK2 and Floxed mice. **f** Representative immunoblots of total and biotinylated surface proteins from primary hippocampal cells isolated from Floxed, CMV and CaMK2 mice revealed with either anti-P2X4, anti-RFP or both antibodies, respectively. As in E, total proteins of P2X4KO macrophages were used as a negative control. **g** Quantification of surface/total P2X4WT and P2X4mCherryIN in hippocampal cells. Bars represent mean ± s.e.m. of the surface/total ratio of P2X4WT (grey bar) in Floxed and CaMK2 mice and P2X4mCherryIN in CaMK2 (orange bar) or CMV mice (red bar) and show that P2X4 surface expression is strongly increased in cells expressing P2X4mCherryIN mice compared to those expressing P2X4WT. The number of independent experiments is indicated by circles. one-way ANOVA, and Bonferroni's post hoc test, $F(3, 20) = 17.2$; * $p < 0.05$, ** $p < 0.01$, *** $p < 0.001$.

**Fig. 5** Surface increase of neuronal P2X4 impairs LTP and LTD at CA1 hippocampal synapses and alters anxiety, spatial learning and memory. **a** Schematic drawing of the experimental protocol and example of a fEPSP recorded from the hippocampal CA1 region (Erec). fEPSP were induced by the electrical stimulation (stim) of the Schaffer collaterals (Sch) in the CA3 area and recorded in the stratum radiatum layer in brain slices of Floxed, CaMK2 and CMV P2X4mCherryIN mice. DG: dentate gyrus. **b** The relative field slope is plotted against stimulation intensity. The input/output curves for neurons in hippocampal slices from Floxed (gray circles, n = 7), CaMK2 (orange circles, n = 7) and CMV P2X4mCherryIN (red circles, n = 6) mice show similar linear regression (mean ± s.e.m., one-way ANOVA, $F(2,18) = 0.15$; $p = 0.85$) indicating that basal synaptic transmission is not affected by the increase of surface P2X4 expression. **c,d** Surface P2X4 increase impairs LTP. **c** Plots of normalized fEPSP slopes recorded in CA1 over time before and after the induction of LTP. LTP was induced by 3 tetanic trains (100Hz, 1s) with a 20 sec interval) in control Floxed (n = 10), CaMK2 (n = 10) or CMV mice (n = 9). **d** Bar graph summary showing the relative change of fEPSP slope 30-40 min after the induction of LTP in Floxed (144.7 ± 11.3% of baseline, n = 10), CMV mice (113.2 ± 5.27% of baseline, n = 9) or CaMK2 (115.6 ± 3.25% of baseline, n = 10), one-way ANOVA and tuckey's post hoc test; $F(3,25) = 9,41$; $p = 0.002$, *** $p < 0.001$;. Error bars: s.e.m.; number of mice is indicated in parentheses. **e,f**

858 Increased surface P2X4 impairs LTD. **e** Plots of normalized fEPSP slopes recorded in CA1 over the
859 time before and after the induction of LTD with a 1 Hz, 15 min train Floxed (n = 21), CaMK2 (n= 11) and
860 CMV mice (n = 9). **f** Bar graph summary showing the relative change of fEPSP slope 30-40 min after
861 the induction of LTD in Floxed (79.09 ± 3.63% of the baseline, n = 22, $p < 0.001$), CMV (84.58 ± 5.97%
862 of baseline, n = 8, $p > 0.05$) and CaMK2 mice (94.24 ± 3.89% of baseline, n = 9, $p > 0.05$). one-way
863 ANOVA and tuckey's post hoc test; $F(3,44) = 5.44$; $p = 0.0028$, $^{**}p < 0.01$; Error bars: s.e.m.; Number
864 of mice is indicated in parentheses. **g-i** Open field assessments of control (Floxed mice, n= 24) and
865 CaMK2 (n = 13) or CMV (n = 12) P2X4mCherryIN mice. **g** Examples of exploration trajectories (top
866 view) in the empty arena for each type of mice. Peripheral and central activities are indicated by yellow
867 and red traces, respectively. **h** Similar total travel distance by each mouse line in the empty arena during
868 10 min was similar. **i** CaMK2 mice spent more time in the central arena compared to Floxed and CMV
869 mice, one-way ANOVA and Bonferroni's post hoc test; $F(2,46) = 5.139$; $p = 0.0097$, $^{**}p < 0.01$. **j-l** One
870 object exploration test in control (Floxed mice, n= 24) and CaMK2 (n = 13) or CMV (n = 12)
871 P2X4mCherryIN mice. **j** Examples of exploration trajectories (top view) for each type of mice. Activities
872 far away or at proximity of the object are indicated in yellow or red, respectively. **k** Latency to first
873 interaction with the novel object is shown for each type of mouse. One-way ANOVA and Bonferroni's
874 post hoc test, $F(2,46) = 2.868$; $p = 0.067$. **l** CaMK2 mice spent more time exploring the novel object than
875 Floxed and CMV mice. One-way ANOVA, $F(2,46) = 10.27$; $p = 0.0002$; $^{**}p < 0.01$, $^{***}p < 0.001$. **m**
876 Mean percent of time spent in the open arms of the elevated plus maze for Floxed mice (n= 22), CaMK2
877 (n = 14) and CMV (n = 11) mice. CaMK2 spent more time in the open arms, indicating reduced anxiety
878 compared to the other mouse lines. One-way ANOVA and Bonferroni's post hoc test, $F(2,44) = 5.186$;
879 $p = 0.0095$; $^{*}p < 0.05$. **n** Spatial recognition memory evaluated in the Y-maze. Floxed (n= 24), CaMK2
880 (n = 13) or CMV (n = 12) mice were able to recognize the novel arm of the maze that was rendered
881 accessible 4 h after encoding (one-way ANOVA, $F(2,46)=0.097$; $p = 0.907$). **o,p** Spatial learning and
882 memory assessment using the 8-radial maze in Floxed mice (gray), CaMK2 (orange) and CMV (red)
883 mice. The number of mice in each group is indicated in parentheses. **o** Learning occurred over one
884 single day and consisted of 4 blocks of six trials separated by a 1 h interval. The location of the 3

885 constantly baited arms of the maze is indicated in red. CaMK2 mice committed more reference memory
886 errors (visits to unbaited arms) compared to Floxed and CMV mice. *p < 0.05, ** p < 0.01. Paired two-
887 way ANOVA and Bonferroni's post hoc test, Time effect, F(3,255) = 205.3, p < 0.0001. Paired two-way
888 ANOVA, genotype effect, F(2,85) = 4,927, p = 0.0094. **p** Retrieval testing 1 (recent) or 14 (long-term)
889 days after initial training in the 8-arm radial maze for all three mouse lines. Performance achieved on
890 the fourth training block (D0) is shown for comparison. The poorer performance exhibited by CaMK2
891 mice (higher number of errors) was not exacerbated by the passage of time. *p < 0.05, paired two-way
892 ANOVA and Bonferroni's post hoc test, delay effect, F(1,35) = 11.70; p=0.0016. All data are presented
893 as mean ± s.e.m.
894
895
896

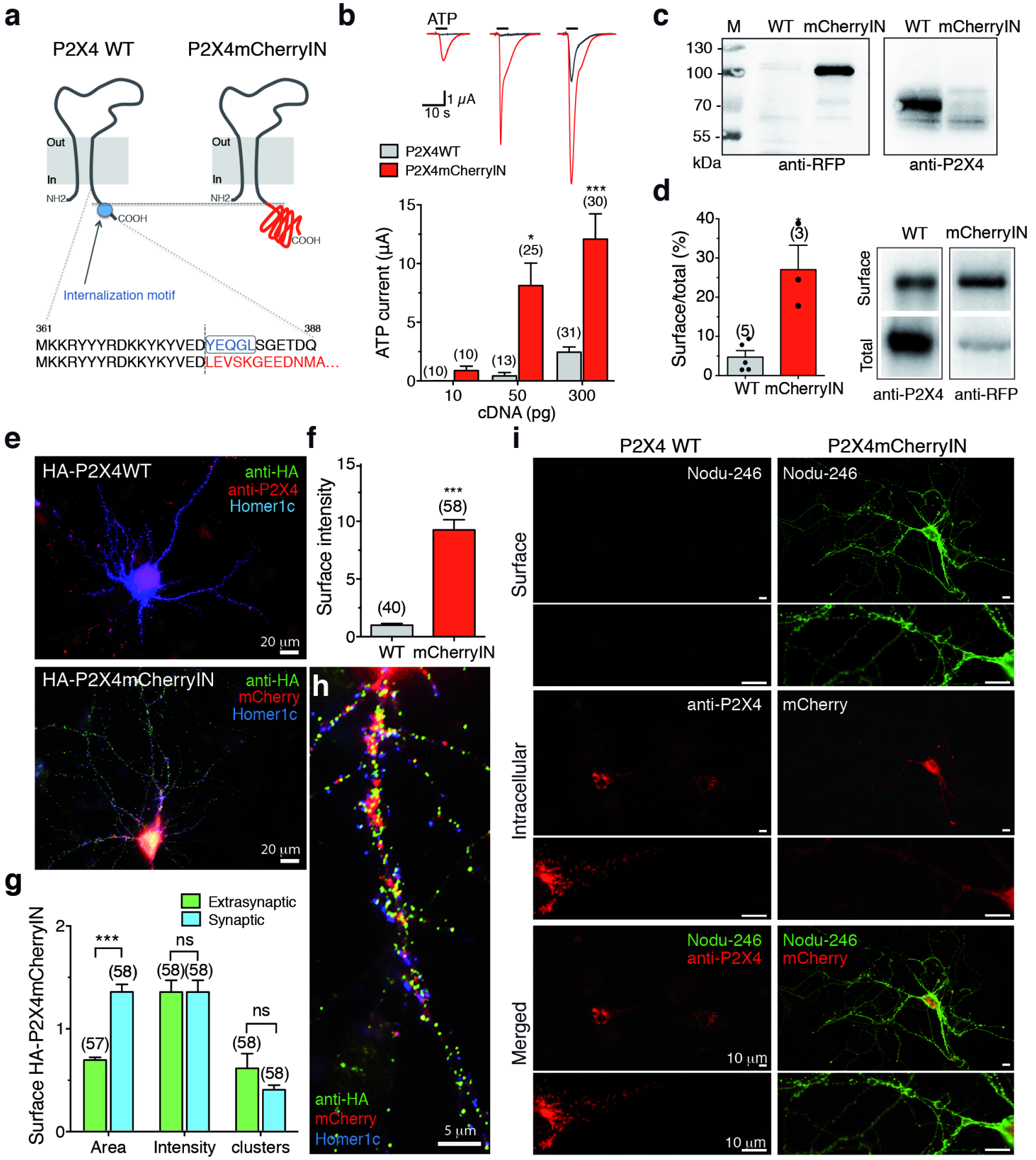
a
P2X4 WT
P2X4mCherryIN
Out
In
NH2
COOH
Internalization motif
361
388
MKKRYYYRDKKYKYVEDYEQGLSGETDQ
MKKRYYYRDKKYKYVEDLEVSKGEEDNMA...
b
ATP
1 μA
10 s
P2X4WT
P2X4mCherryIN
ATP current (μA)
cDNA (pg)
10
50
300
c
M
WT
mCherryIN
WT
mCherryIN
130
100
70
55
kDa
anti-RFP
anti-P2X4
d
Surface/total (%)
WT
mCherryIN
Surface
Total
anti-P2X4
anti-RFP
e
HA-P2X4WT
anti-HA
anti-P2X4
Homer1c
20 μm
HA-P2X4mCherryIN
anti-HA
mCherry
Homer1c
20 μm
f
Surface intensity
WT
mCherryIN
g
Extrasynaptic
Synaptic
Surface HA-P2X4mCherryIN
Area
Intensity
clusters
ns
h
anti-HA
mCherry
Homer1c
5 μm
i
P2X4 WT
P2X4mCherryIN
Surface
Intracellular
Merged
Nodu-246
anti-P2X4
mCherry
10 μm

Fig. 1

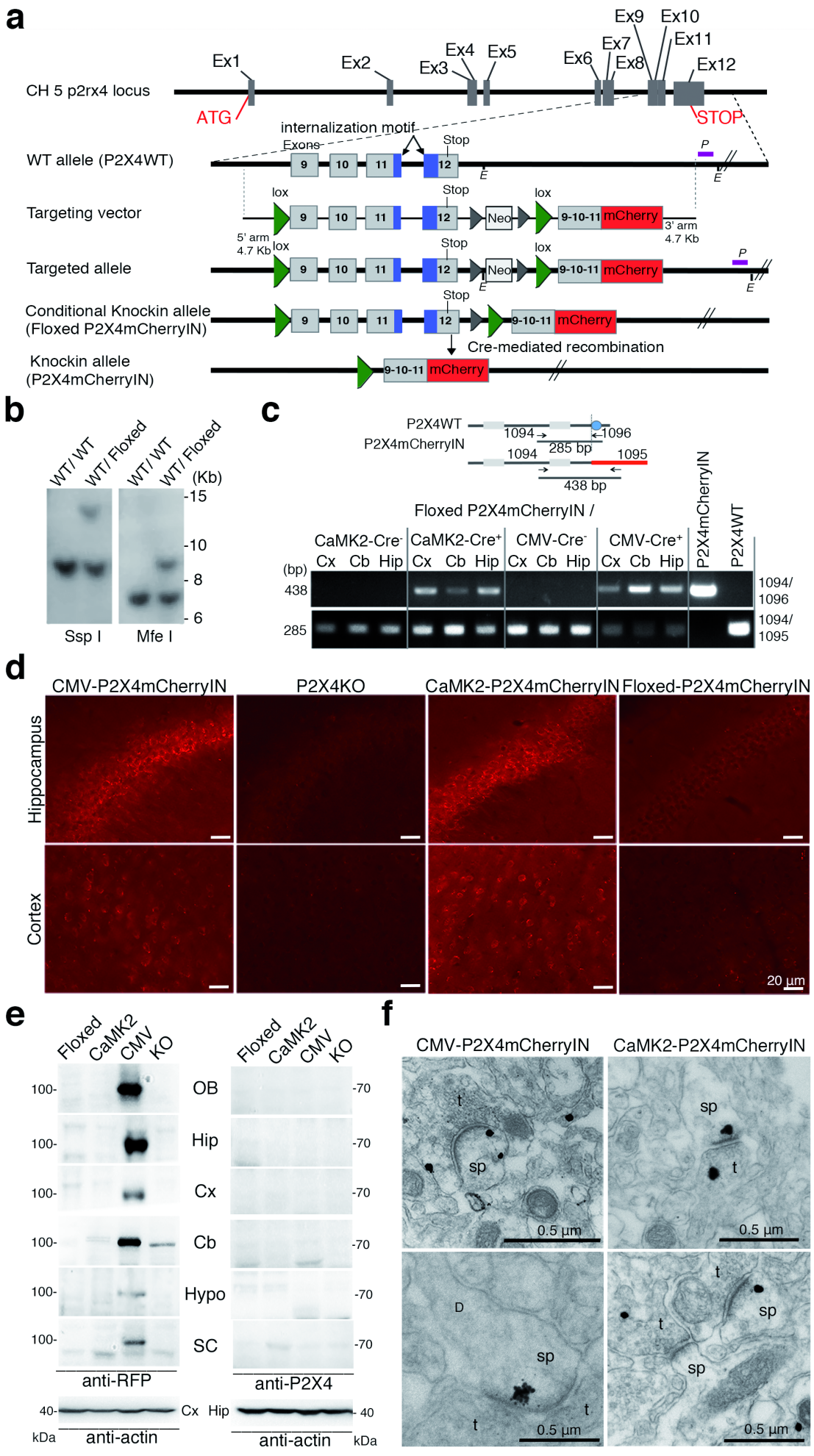
a
CH 5 p2rx4 locus
Ex1
Ex2
Ex3
Ex4
Ex5
Ex6
Ex7
Ex8
Ex9
Ex10
Ex11
Ex12
ATG
STOP
internalization motif
WT allele (P2X4WT)
Exons
Stop
Targeting vector
lox
Neo
9-10-11 mCherry
5' arm 4.7 Kb
3' arm 4.7 Kb
Targeted allele
Conditional Knockin allele (Floxed P2X4mCherryIN)
Cre-mediated recombination
Knockin allele (P2X4mCherryIN)
b
WT/ WT
WT/ Floxed
(Kb)
15
10
8
6
Ssp I
Mfe I
c
P2X4WT
P2X4mCherryIN
1094
1096
285 bp
1095
438 bp
Floxed P2X4mCherryIN /
CaMK2-Cre-
CaMK2-Cre+
CMV-Cre-
CMV-Cre+
Cx Cb Hip
(bp)
438
285
1094/ 1096
1094/ 1095
d
CMV-P2X4mCherryIN
P2X4KO
CaMK2-P2X4mCherryIN
Floxed-P2X4mCherryIN
Hippocampus
Cortex
20 μm
e
Floxed
CaMK2
CMV
KO
OB
Hip
Cx
Cb
Hypo
SC
100-
-70
anti-RFP
anti-P2X4
40-
anti-actin
kDa
f
CMV-P2X4mCherryIN
CaMK2-P2X4mCherryIN
t
sp
D
0.5 μm

Fig. 2

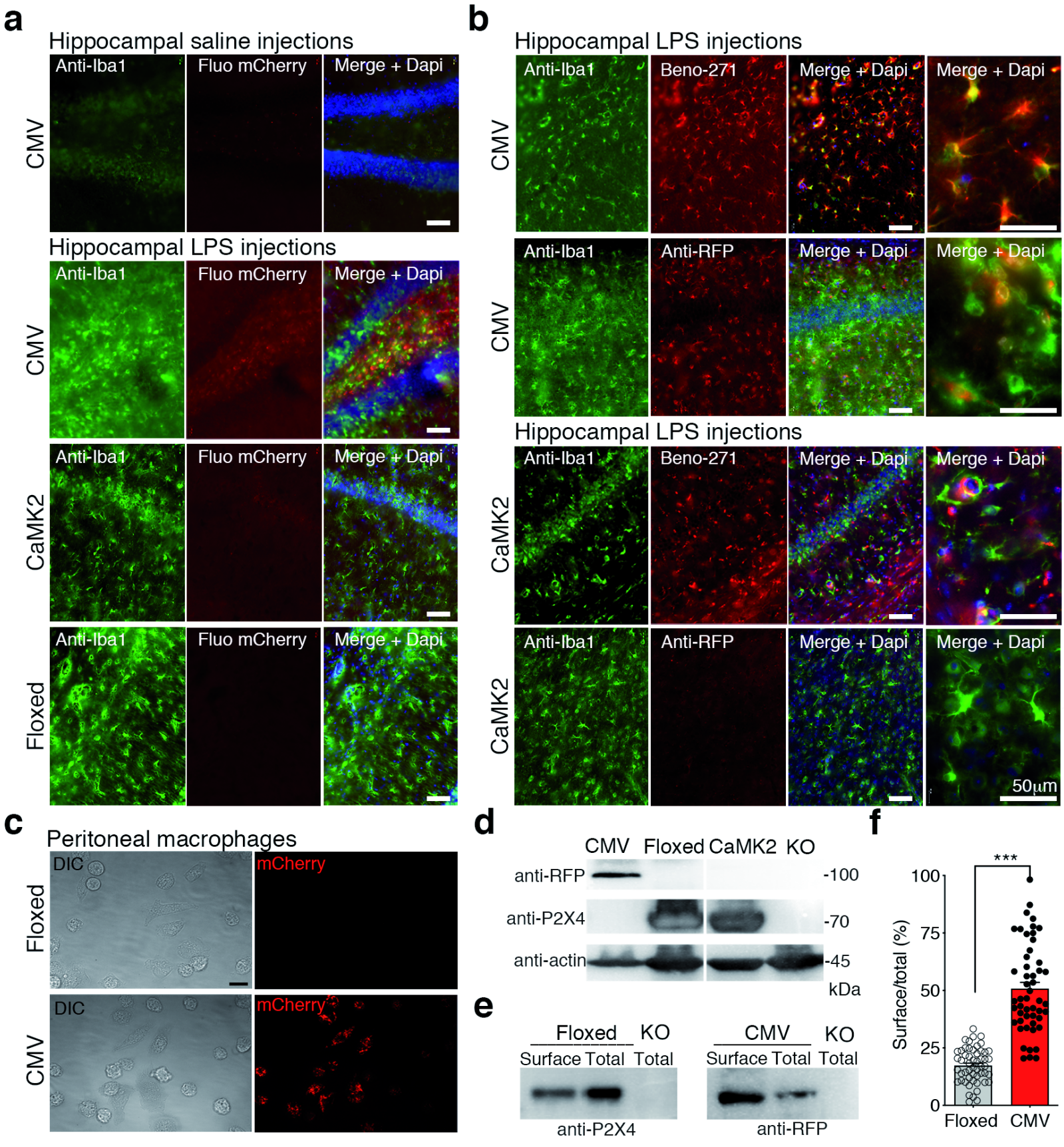
a
Hippocampal saline injections
Anti-Iba1
Fluo mCherry
Merge + Dapi
CMV
Hippocampal LPS injections
Anti-Iba1
Fluo mCherry
Merge + Dapi
CMV
CaMK2
Floxed
b
Hippocampal LPS injections
Anti-Iba1
Beno-271
Anti-RFP
Merge + Dapi
CMV
CaMK2
50µm
c
Peritoneal macrophages
DIC
mCherry
Floxed
CMV
d
CMV
Floxed
CaMK2
KO
anti-RFP
anti-P2X4
anti-actin
-100
-70
-45
kDa
e
Floxed
KO
Surface
Total
Total
anti-P2X4
CMV
KO
Surface
Total
Total
anti-RFP
f
***
Surface/total (%)
100
75
50
25
0
Floxed
CMV

Fig. 3

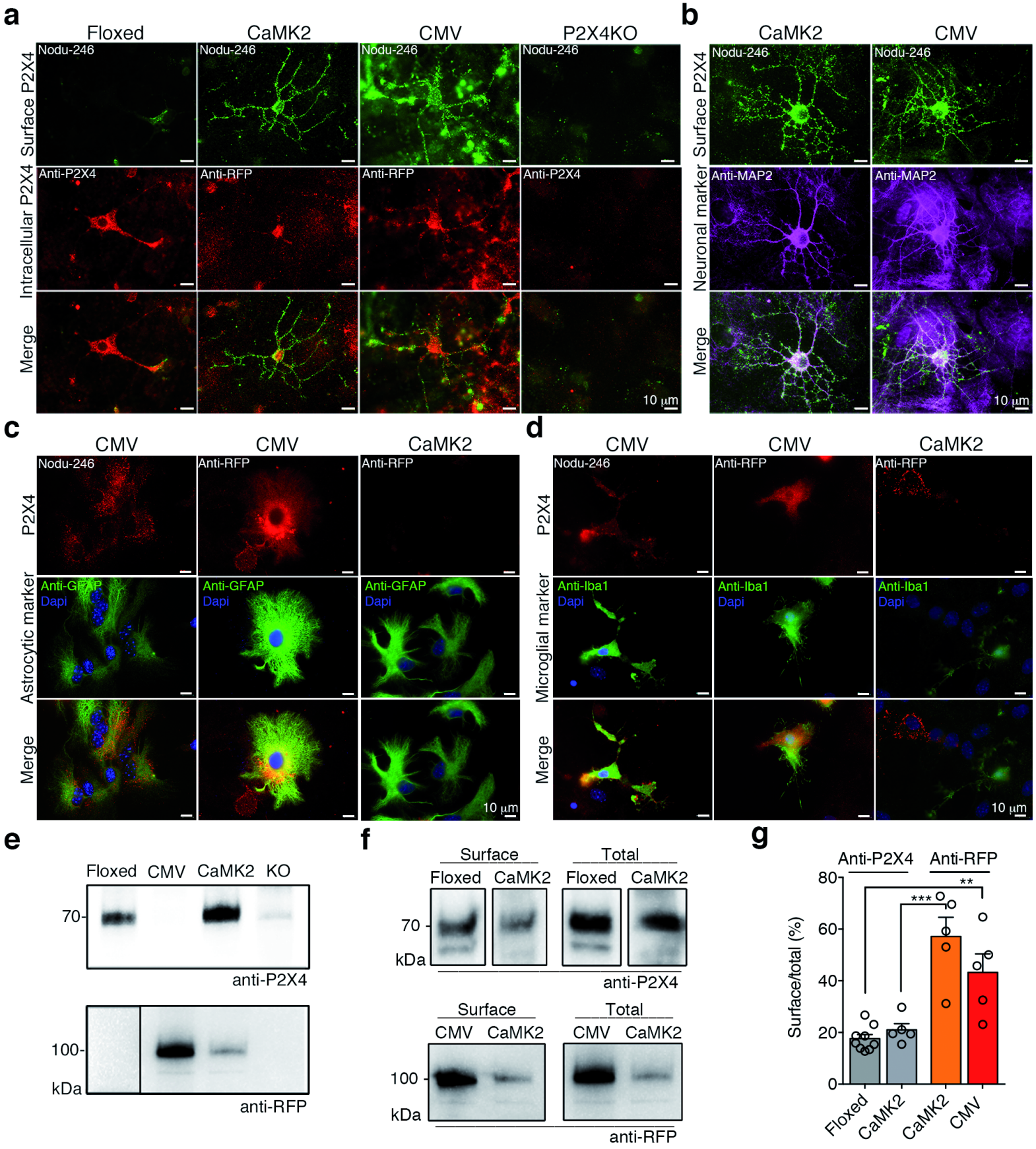
a
Floxed
CaMK2
CMV
P2X4KO
Surface P2X4
Intracellular P2X4
Merge
Nodu-246
Anti-P2X4
Anti-RFP
10 μm
b
CaMK2
CMV
Neuronal marker
Anti-MAP2
c
CMV
CaMK2
P2X4
Astrocytic marker
Anti-GFAP
Dapi
d
Microglial marker
Anti-Iba1
e
Floxed
CMV
CaMK2
KO
70
100
kDa
anti-P2X4
anti-RFP
f
Surface
Total
g
Anti-P2X4
Anti-RFP
Surface/total (%)
***
**

Fig. 4

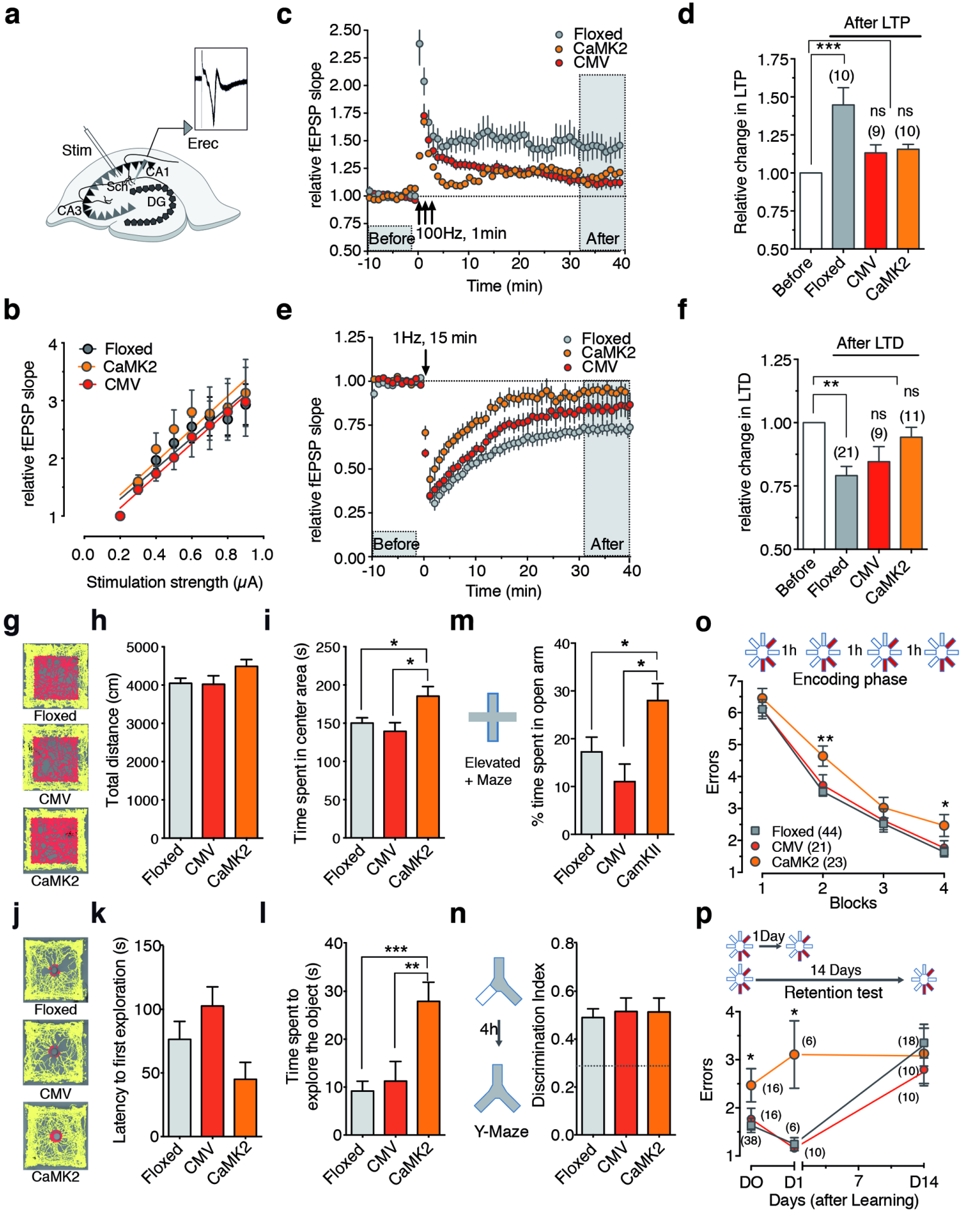
a
Stim
Erec
CA1
Sch
DG
CA3
b
Floxed
CaMK2
CMV
relative fEPSP slope
Stimulation strength (μA)
c
Floxed
CaMK2
CMV
relative fEPSP slope
100Hz, 1min
Before
After
Time (min)
d
After LTP
***
(10)
ns
(9)
ns
(10)
Relative change in LTP
Before
Floxed
CMV
CaMK2
e
1Hz, 15 min
Floxed
CaMK2
CMV
relative fEPSP slope
Before
After
Time (min)
f
After LTD
**
ns
ns
(21)
(9)
(11)
relative change in LTD
Before
Floxed
CMV
CaMK2
g
Floxed
CMV
CaMK2
h
Total distance (cm)
Floxed
CMV
CaMK2
i
Time spent in center area (s)
Floxed
CMV
CaMK2
m
Elevated
+ Maze
% time spent in open arm
Floxed
CMV
CamKII
o
1h
1h
1h
Encoding phase
Errors
Floxed (44)
CMV (21)
CaMK2 (23)
Blocks
j
Floxed
CMV
CaMK2
k
Latency to first exploration (s)
Floxed
CMV
CaMK2
l
Time spent to explore the object (s)
Floxed
CMV
CaMK2
n
4h
Y-Maze
Discrimination Index
Floxed
CMV
CaMK2
p
1Day
14 Days
Retention test
Errors
DO
D1
7
D14
Days (after Learning)

Fig. 5